PCCP

PAPER

View Article Online
View Journal | View Issue

Cite this: *Phys. Chem. Chem. Phys.*, 2016, **18**, 3234

The role of hydrogen during Pt–Ga nanocatalyst formation†

Matthias Filez,[a] Evgeniy A. Redekop,[a] Vladimir V. Galvita,[a] Hilde Poelman,*[a] Maria Meledina,[b] Stuart Turner,[b] Gustaaf Van Tendeloo,[b] Alexis T. Bell[c] and Guy B. Marin[a]

Received 28th November 2015,
Accepted 4th January 2016

DOI: 10.1039/c5cp07344h

www.rsc.org/pccp

Hydrogen plays an essential role during the *in situ* assembly of tailored catalytic materials, and serves as key ingredient in multifarious chemical reactions promoted by these catalysts. Despite intensive debate for several decades, the existence and nature of hydrogen-involved mechanisms – such as hydrogen-spillover, surface migration – have not been unambiguously proven and elucidated up to date. Here, Pt–Ga alloy formation is used as a probe reaction to study the behavior and atomic transport of H and Ga, starting from Pt nanoparticles on hydrotalcite-derived Mg(Ga)(Al)O_x supports. *In situ* XANES spectroscopy, time-resolved TAP kinetic experiments, HAADF-STEM imaging and EDX mapping are combined to probe Pt, Ga and H in a series of H_2 reduction experiments up to 650 °C. Mg(Ga)(Al)O_x by itself dissociates hydrogen, but these dissociated hydrogen species do not induce significant reduction of Ga^{3+} cations in the support. Only in the presence of Pt, partial reduction of Ga^{3+} into $Ga^{\delta+}$ is observed, suggesting that different reaction mechanisms dominate for Pt- and Mg(Ga)(Al)O_x-dissociated hydrogen species. This partial reduction of Ga^{3+} is made possible by Pt-dissociated H species which spillover onto non-reducible Mg(Al)O_x or partially reducible Mg(Ga)(Al)O_x and undergo long-range transport over the support surface. Moderately mobile $Ga^{\delta+}O_x$ migrates towards Pt clusters, where $Ga^{\delta+}$ is only fully reduced to Ga^0 on condition of immediate stabilization inside Pt–Ga alloyed nanoparticles.

Introduction

Supported metallic nanoparticles[1–5] are widely employed in energy storage, catalysis, and environmental management. Currently, multiple methods are being developed for atomic tailoring of these nanostructured materials with unprecedented precision. Examples include atomic layer deposition (ALD)[6,7] and shape-controlled synthesis,[8] techniques which offer an ever-increasing control of the nanoparticle morphology and thereby yield superior functional properties. However, these methods are often prohibitively expensive for production in industrially relevant quantities. Instead, commercial manufacturing of nanostructured materials typically relies on bulk synthesis methods such as deposition–precipitation and incipient wetness impregnation, which are based on the thermodynamically or kinetically controlled ordering of elements within the material.[9]

In recent years, a family of materials derived from bulk synthesized layered double hydroxides (LDHs) has emerged as versatile catalysts,[10–13] electrocatalysts,[14] photocatalysts,[15] chemical storage materials,[16] and drug delivery agents.[17] To produce mono- or bimetallic heterogeneous catalysts, multiple metal ions are first incorporated into the framework of a LDH precursor during a scalable and inexpensive synthesis procedure.[18] The LDH structure is then collapsed by high-temperature oxidation (calcination), forming a thermally stable non-reducible metal oxide support which contains and exposes reducible isolated metal ions or very small oxidized metal clusters. Upon subsequent high-temperature H_2 reduction, the incorporated metal ions reduce and assemble into well-dispersed (multi-)metallic nanoparticles on the support surface. Alternatively, active metals may be deposited onto the LDH-derived supports *via* conventional impregnation techniques, as in the well-described Pt–Sn/Mg(Al)O_x system.[19–22] Since many applications for LDH-derived materials have already emerged, with more expected to come, deeper insight into their chemistry is highly desirable.

[a] *Laboratory for Chemical Technology (LCT), Ghent University, Technologiepark 914, B-9052 Ghent, Belgium. E-mail: hilde.poelman@ugent.be; Fax: +00 32 9 264 49 99; Tel: +00 32 9 331 17 22*

[b] *Electron Microscopy for Materials Science (EMAT), University of Antwerp, Groenenborgerlaan 171, B-2020 Antwerp, Belgium*

[c] *University of California, Berkeley, CA 94720, USA*

† Electronic supplementary information (ESI) available: Ga K edge XANES quantitative peak fitting analysis procedure, Ga K edge EXAFS modeling of Pt/Mg(Ga)(Al)O_x before H_2 TPR, possible Ga–H bond formation and Ga coordination change and their influence on the Ga K edge XANES edge, Ga K edge XANES reference spectra, TAP experimental details and data analysis procedure, XANES during H_2 TPR to 750 °C on a physical mixture of Pt/Mg(Al)O_x and Mg(Ga)(Al)O_x. See DOI: 10.1039/c5cp07344h

The collapse of the LDH structure during calcination treatment is typically accompanied by complex processes, including the removal of CO_2, H_2O and residual organic ligands, that have been extensively characterized.[23,24] However, the mechanisms and driving forces acting during H_2 reduction[25] and leading to the formation of high-performing multi-metallic nanoparticles are not well-established. These formation mechanisms involve highly concerted actions of convoluted atomic scale processes including the migration of metal atoms and ions, reactions of hydrogen, alloying and phase transitions. In fact, these events determine the catalytic properties of the resulting nanostructured catalyst under operating conditions, as they induce subtle changes in the distribution of constituent elements at the catalytic surface. For this reason, the facile *in situ* formation of these specific active sites should be investigated in order to rationally design synthesis and pre-treatment protocols and better predict the precise *operando* catalyst nanostructure and performance.

Hydrogen spillover (H-spillover) is an important mechanism in catalysis which may control the reduction behavior and catalytic activity of LDH-derived metallic catalysts. Several studies have invoked H-spillover to explain the enhancement of cation reduction from the calcined LDH framework by the presence of other metals on the surface, which serve as hydrogen activators.[26,27] However, unambiguous evidence of the spillover phenomenon in LDH-derived materials is lacking, and H-spillover onto non-reducible supports such as MgO is still a matter of intense debate.[28–30] It is unclear to what degree the observations attributed to spillover can be explained by the mobility of H_2-dissociating metal species over the support surface, since the spatial range of metal mobility in these materials has not been systematically characterized. Im *et al.* constructed a sophisticated model catalyst featuring Pt nanoparticles embedded deeply within an aluminosilicate matrix.[31] The absence of extra-framework Pt in their catalyst system was confirmed by chemisorption measurements and the only molecule small enough to diffuse towards Pt was H_2. Using this model catalyst with guaranteed absence of metal transport, hydrogenation reactions at the zeolite external surface involving only the hydrogen spilled-over from embedded Pt and migrated to the surface could be studied. Such model systems are, however, rare and not available for LDH-derived supports.

Here, both the migration of metal atoms and the involvement of H-spillover are examined during the formation of highly active and selective Pt–Ga/Mg(Ga)(Al)O_x dehydrogenation catalysts from calcined Mg,Ga,Al-LDH precursors (Mg(Ga)(Al)O_x) decorated with Pt nanoparticles. In addition to the significant industrial relevance of Pt–Ga catalysts in general,[32,33] these specific materials present a convenient fundamental model system for studying H-spillover and nano-alloying in catalysis. Recently, a comprehensive characterization of these catalysts as well as their Pt–In and Pt–Sn analogs has been performed by our group[22,34–40] and others.[19–21,41] The reduction of framework Ga^{3+} is a highly-activated process, characterized by much higher transition temperatures than the reduction of other reducible metal ions such as Cu and Ni[42] or Pd and Zn[26] in LDH-derived frameworks. Consequently, Pt deposited on a Mg(Ga)(Al)O_x support provides a sensitive model for examining the processes that could lower the activation energy for Ga^{3+} reduction, such as Ga migration towards Pt or H-spillover.

Experimental section

Catalyst synthesis

Mg(Al)O_x and Mg(Ga)(Al)O_x supports were synthesized by employing the co-precipitation routine reported by Sun *et al.*[34] For the production of Mg(Al)O_x, an aqueous solution of $Mg(NO_3)_2{\cdot}6H_2O$ (Sigma-Aldrich, 98–102%) and $Al(NO_3)_3{\cdot}9H_2O$ (Sigma-Aldrich, 98.5%) was mixed with an aqueous solution of Na_2CO_3 (EMD Chemicals Inc., 99.5%) and NaOH (Fisher Scientific, 98.3%). For the synthesis of Mg(Ga)(Al)O_x, $Ga(NO_3)_3{\cdot}xH_2O$ (Sigma-Aldrich, 99.99%) was added to the aqueous solution in addition to the components listed for the production of Mg(Al)O_x. After room temperature aging during 24 h, the precipitated support material was filtered, washed with deionized water until pH 7, and dried at 110 °C. The resulting hydrotalcite-like material (pure Mg,Al-HT and Ga-incorporated Mg,Ga,Al-HT) was then calcined in air for 4 h at 650 °C, leading to a mixed oxide (Mg(Al)O_x and Mg(Ga)(Al)O_x).

Pt deposition on these supports consisted of incipient wet impregnation of a toluene (Sigma-Aldrich, 99.9%) - $Pt(acac)_2$ (Sigma-Aldrich, 99.99%) solution on Mg(Al)O_x and Mg(Ga)(Al)O_x. Next, toluene was evaporated by heating the material at 110 °C. A calcination treatment to 650 °C in air was performed in order to decompose the precursor ligands and allow Pt nanoparticle formation on the support surface, labeled as 'Pt/Mg(Al)O_x' and 'Pt/Mg(Ga)(Al)O_x'.

XANES

In situ XAS measurements were executed at the Pt L_{III} edge (11 564 eV) using the DUBBLE beam line[43] of the ESRF synchrotron (6 GeV, current 160–200 mA, Grenoble – France). The prepared material were introduced into a 2 mm quartz capillary and fixed with quartz wool plugs. This capillary was then connected to gas lines by swagelok® fittings and subsequently mounted below the gas blower (FMB Oxford). The DUBBLE gas rig system was employed to regulate the gas flows through the capillary.[44] Optics alignment and energy referencing was performed using a Pt foil and W reference. XANES measurements (±5 min per spectrum) were recorded in transmission mode. XAS data analysis was executed by using the Demeter 0.9.13 software package.[45] Background subtraction and subsequent normalization were performed by employing the methodology of Koningsberger *et al.*[46]

HAADF-STEM imaging and EDX mapping

HAADF-STEM imaging and EDX mapping were carried out on a FEI Tecnai Osiris microscope, equipped with a ''Super-X'' four quadrant EDX detector for EDX mapping, operated at 200 kV acceleration voltage.

Temporal analysis of products (TAP) experiments

Each sample was loaded into the TAP microreactor as a thin zone located between two larger, inert zones packed with quartz.

The tip of the internal thermocouple was placed inside the sample zone. The sample was first reduced for 20 minutes in a flow of H_2 at 650 °C and then evacuated for 20 minute to the background pressure of 10^{-7} Torr. After evacuation, a series of H_2/He (1 : 1) pulses was introduced into the microreactor by firing an electro-magnetically-driven pulse-valve (feed pressure 2.2 bar, driving voltage 18 V). Pulse width was kept at 90 μs. The exit-flow rate was monitored every millisecond with a calibrated Extrel QMS. Further experimental characteristics and the TAP data analysis procedure are respectively listed (Table S1) and described in the ESI.†

Results and discussion

To obtain evidence of the spillover phenomena and to simultaneously determine how far Ga species travel within the support during catalyst formation, *in situ* XAS measurements at both the Pt L_{III} and Ga K edges (Fig. 1) were performed during a temperature-programmed reduction treatment (H_2 TPR over 25–650 °C, 0.2 °C s^{-1}, 5% H_2/He) for the following four materials: (i) the actual bimetallic Pt/Mg(Ga)(Al)O_x catalyst, (ii) the parent Pt-free support material Mg(Ga)(Al)O_x, (iii) a Ga-free monometallic Pt/Mg(Al)O_x catalyst with comparable Pt content, and (iv) a physical mixture of the Pt-free support Mg(Ga)(Al)O_x and the Ga-free catalyst Pt/Mg(Al)O_x, *i.e.* (iv) = (ii) + (iii). All materials were calcined for 4 hours in air at 650 °C prior to the TPR procedure. The details of XAS measurements and data analysis can be found in the Methods section.

During TPR, the XANES spectra at the Pt L_{III} edge of the Pt/Mg(Ga)(Al)O_x catalyst exhibit two characteristic trends (Fig. 1f): the white line intensity decreases and the edge shifts to higher energies.[36,39,40] The white line intensity decreases due to Pt reduction, as confirmed by the reduction of Ga-free Pt/Mg(Al)O_x reference (Fig. 1d), while the edge shifts due to Pt–Ga alloying.[39] Hsu *et al.*[47] and Giedigkeit *et al.*[48] observed a similar Pt L_{III} edge shift for $PtGa_2$ alloys. Bus and van Bokhoven[49] reported that electron donation from Au to Pt during PtAu

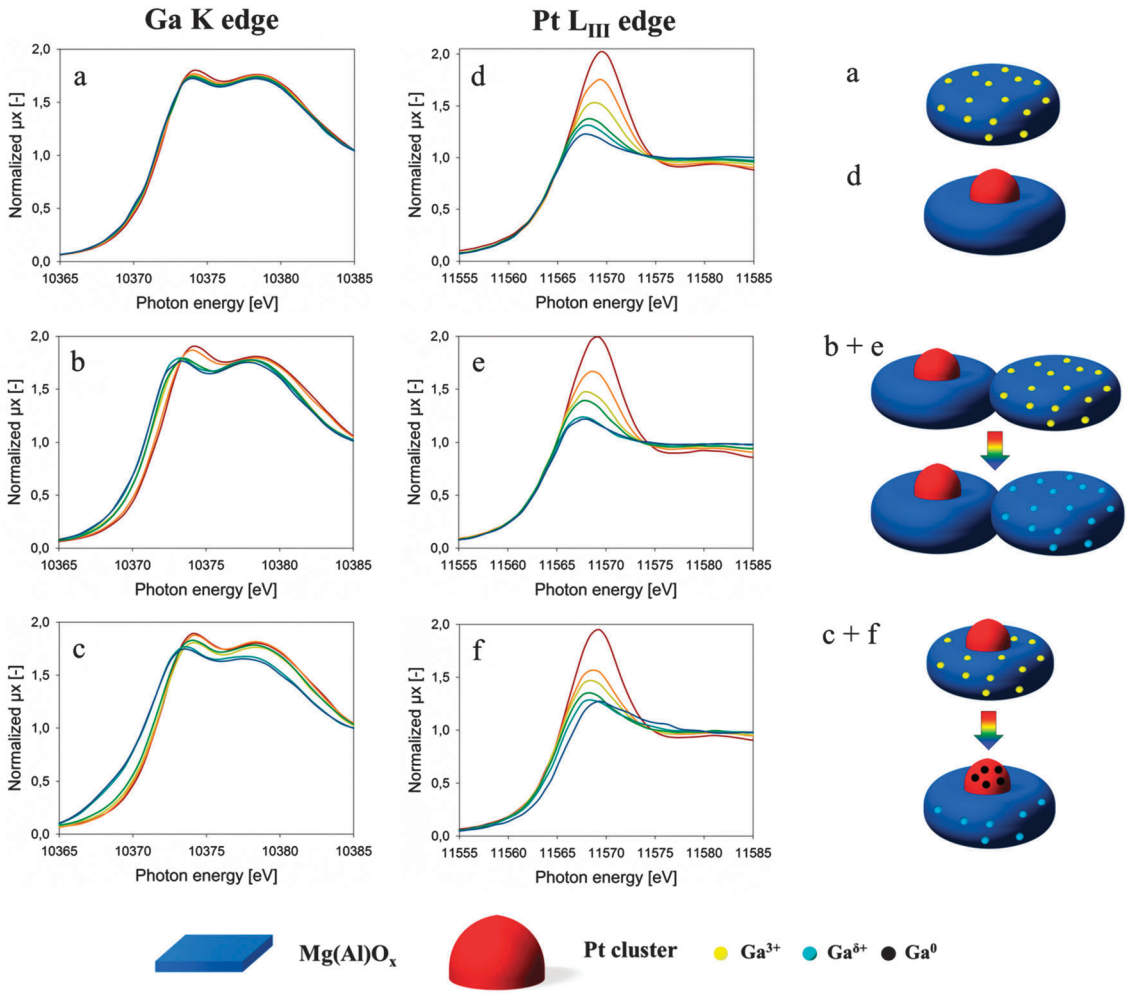

Fig. 1 Ga K edge XANES spectra recorded during H_2/He TPR to 650 °C of (a) Mg(Ga)(Al)O_x, (b) physical mixture of Pt/Mg(Al)O_x + Mg(Ga)(Al)O_x and (c) Pt/Mg(Ga)(Al)O_x; Pt L_{III} edge XANES spectra recorded during H_2/He TPR to 650 °C of (d) Pt/Mg(Al)O_x, (e) physical mixture of Pt/Mg(Al)O_x + Mg(Ga)(Al)O_x and (f) Pt/Mg(Ga)(Al)O_x. During TPR, the recorded spectra evolve from red (start) towards blue (end). All plots are provided with a representation of the materials before and after reduction.

alloying results in a positive edge shift at the Pt L_{III} edge. Since Ga is less electronegative than Pt (Ga: 1.81, Pt: 2.28), charge transfer from Ga to Pt is likely to occur, leading to the observed edge shift. This electron transfer results in stabilization of Pt–Ga bonds and Pt–Ga alloying, as observed after TPR of Pt/Mg(Ga)(Al)O_x (Fig. 1f).

During TPR, the complementary Ga K edge XANES spectra exhibit decreasing white line intensity in addition to an edge shift to lower energies (Fig. 1c). In order to quantitatively allocate these spectral changes, peak fitting analysis is performed on the initial and final Ga K edge XANES spectra respectively before (Fig. 2a) and after (Fig. 2b) H_2 TPR of Pt/Mg(Ga)(Al)O_x. Each XANES contribution is modeled by an arctangent for continuum absorption and a Gaussian for the white line, the former being scaled proportional to the Gaussian peak intensity (following Nishi *et al.*,[50] see ESI†). The Ga XANES spectrum before H_2 TPR of Pt/Mg(Ga)(Al)O_x consists of two distinct contributions (Fig. 2a): (1) tetrahedrally oxygen coordinated Ga^{3+} cations (first peak above the edge, Ga^{3+}(t)) and (2) octahedrally oxygen coordinated Ga^{3+} (second peak above the edge, Ga^{3+}(o)). As observed in Fig. 2a, Ga^{3+}(t) is most abundant relative to Ga^{3+}(o). Indeed, the ratio of Gaussian peak intensities of tetrahedral to octahedral Ga^{3+} (Ga^{3+}(t)/Ga^{3+}(o)) amounts to 1.5, implying that 60% of the Ga^{3+} cations have tetrahedral oxygen coordination whereas the remaining 40% consists of octahedral Ga^{3+}.[50] Ga K edge EXAFS modeling fully corroborates these XANES results, since a Ga–O coordination number N_{Ga-O} of 4.7 ± 0.8 is obtained (60% × 4O + 40% × 6O = 4.8O on average, see ESI†).

Peak fitting of the Ga XANES spectrum after H_2 TPR of Pt/Mg(Ga)(Al)O_x requires two additional contributions at lower photon energies to be included besides Ga^{3+}(t) and Ga^{3+}(o): (1) a contribution around – 2 eV below the Ga^{3+}(t) peak, responsible for the observed edge shift in the total Ga K edge XANES signal during H_2 TPR, and (2) a contribution around – 5–6 eV below the Ga^{3+}(t) feature, causing a subtle but significant shoulder in the pre-edge region. It should be noted that the Gaussian and arctangent functions of the Ga^{3+}(t) and Ga^{3+}(o) were set at identical energies as compared to their positions in the signal before H_2 TPR of Pt/Mg(Ga)(Al)O_x.

The physical origin of the peak around – 5–6 eV below the Ga^{3+}(t) peak position lies in the formation of metallic Ga^0. Pt L_{III} edge XANES data during H_2 TPR of Pt/Mg(Ga)(Al)O_x

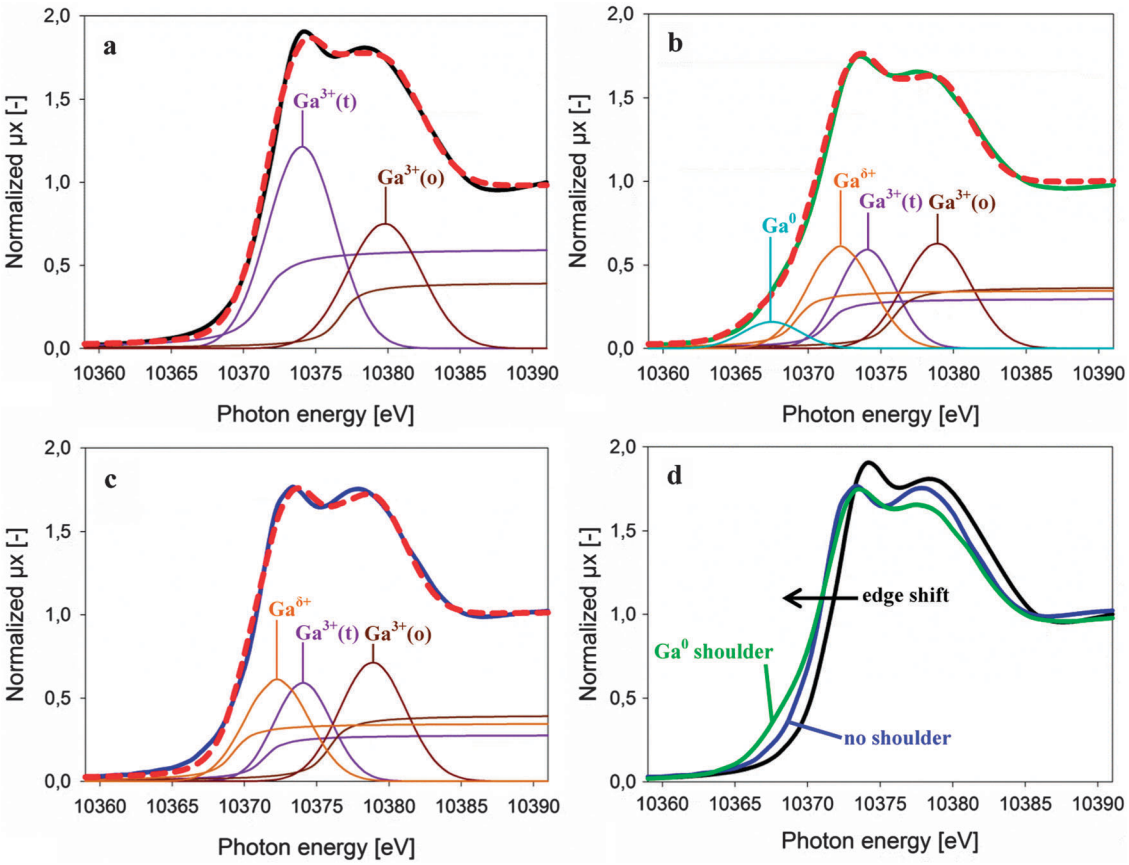

Fig. 2 Ga K edge XANES spectra recorded (a) before (black full line) and (b) after (green full line) H_2 TPR of Pt/Mg(Ga)(Al)O_x to 650 °C, and (c) after H_2 TPR of the physical mixture of Pt/Mg(Al)O_x + Mg(Ga)(Al)O_x (blue full line). The fits to the experimental signal are displayed as dashed red lines. As indicated by the labels, the Ga^{3+}(o), Ga^{3+}(t), $Ga^{\delta+}$ and Ga^0 contributions are depicted as brown, purple, orange and light blue lines, respectively. A contribution consists of a combined Gaussian and arctangent function. (d) is a plot which compares the experimental black, green and blue signals depicted in plots (a), (b) and (c), respectively. As indicated, a clear edge shift is observed for H_2 reduced Pt/Mg(Ga)(Al)O_x (green full line) and Pt/Mg(Al)O_x + Mg(Ga)(Al)O_x (blue full line), relative to non-reduced Pt/Mg(Ga)(Al)O_x (black full line). In addition, a significant shoulder, characteristic for metallic Ga^0 formation is observed for H_2 reduced Pt/Mg(Ga)(Al)O_x (green full line), whereas the latter contribution is absent for H_2 reduced Pt/Mg(Al)O_x + Mg(Ga)(Al)O_x (blue full line).

confirm that part of the Ga atoms are indeed in a metallic Ga^0 state, since Pt–Ga alloying is occurring (Fig. 1f). In addition, negative Ga K edge shifts of ~ -5 to 6 eV were previously observed when Ga_2O_3 is reduced to metallic Ga[51,52] (see also ESI†). Indeed, the reduction of metal oxides generally results in an edge shift towards lower photon energies. This suggests that the peak ~ -2 eV below the Ga^{3+}(t) peak position corresponds to a $Ga^{\delta+}O_x$ intermediate, as the latter contribution is situated at energies intermediate to Ga^0 at the one hand, and Ga^{3+}(t) at the other hand. The occurrence of partially reduced $Ga^{\delta+}O_x$ species at the Mg(Ga)(Al)O_x support surface is supported by multiple studies which report on the formation of Ga_2O as intermediate step during the reduction of Ga_2O_3 into GaH_x or Ga^0.[53–56] Two other phenomena could induce a Ga K edge XANES shift (Fig. 1c), namely (1) Ga–H bond formation and (2) a change in Ga coordination from Ga^{3+}(o) → Ga^{3+}(t).[50,51] However, as explained in the ESI,† these cannot be held responsible for the observed edge shifts in the current study.

Consequently, the observations can be clarified by the partial reduction of Ga^{3+}(t) and/or Ga^{3+}(o) support cations into $Ga^{\delta+}O_x$ species. Such partial Ga^{3+} reduction will shift the Ga K edge XANES edge energy below the one of Ga^{3+}(t) – the lowest edge position for the Ga^{3+} oxidation state. Notably, strong Ga^{3+}(t)/Ga^{3+}(o) contributions remain present in the Ga K edge XANES signal after H_2 TPR of Pt/Mg(Ga)(Al)O_x (Fig. 2b). This suggests that a large fraction of the Ga^{3+}(t) and Ga^{3+}(o) cations are not reduced but rather stabilized as Ga^{3+} cations inside the bulk support during H_2 TPR, while only the surface fraction is being partially reduced. Upon partial reduction of these surface Ga^{3+} cations, only part of the resulting $Ga^{\delta+}$ species fully reduce into metallic Ga^0 and alloy with Pt, as supported by both Ga K and Pt L_{III} edge XANES. To differentiate between the different steps involved in the process of Ga reduction and alloying within these materials, Pt and Ga XANES spectra obtained during the actual catalyst formation were compared to those obtained during the reduction of the Pt-free Mg(Ga)(Al)O_x support (ii) and the physical mixture (iv).

During TPR, the Ga K edge XANES spectra of bare Mg(Ga)(Al)O_x support reveals insignificant changes, implying that negligible Ga reduction occurs below 650 °C on the time scale of the experiment (Fig. 1a). In contrast, the Ga K edge XANES spectra acquired during the H_2 TPR of the physical mixture, *i.e.* Pt/Mg(Al)O_x + Mg(Ga)(Al)O_x, undergo significant changes indicative of partial Ga^{3+} reduction (Fig. 1b): the edge shifts to lower energies and the white line decreases – just like for Pt/Mg(Ga)(Al)O_x. Indeed, quantitative peak fitting analysis shows that partially reduced $Ga^{\delta+}$ species are present besides Ga^{3+}(t) and Ga^{3+}(o), as indicated in Fig. 2c. Hence, the reduction of Ga is promoted in the presence of Pt even when Pt and Ga are located on separate grains. In contrast to H_2 reduced Pt/Mg(Ga)(Al)O_x, no metallic Ga^0 XANES contribution is present around – 5–6 eV below Ga^{3+}(t) for the reduced physical mixture (Fig. 2c). Despite clear signs of Ga reduction within the physical mixture, the absence of the shoulder in its Ga K pre-edge suggests that no or a negligible amount of Ga^0 is formed (Fig. 2d).

The white line of the Pt L_{III} XANES edge also decreases during the reduction of the physical mixture (Fig. 1e), in a similar way to the Ga-free Pt/Mg(Al)O_x reference material and the bimetallic Pt/Mg(Ga)(Al)O_x catalyst. However, the edge does not shift to higher energies, unlike in the case of the bimetallic catalyst. It can be concluded that both Pt and Ga within the physical mixture are reduced without undergoing the long-range transport which could lead to alloying. In combination with XANES results for the bimetallic Pt/Mg(Ga)(Al)O_x catalyst, this observation indicates that the semi-mobile $Ga^{\delta+}$ species on the support are capable of further reduction into Ga^0 at 650 °C, but only if the Ga^0 can be immediately stabilized through formation of an alloy with nearby Pt. It should be noted that contrary to the Ga^{3+} species embedded within the Mg(Ga)(Al)O_x framework, partial reduction of Ga^{3+} in neither bulk[38] nor nano-dispersed[33] Ga_2O_3 into the $Ga^{\delta+}$ species occurs.

The enhancement of Ga reduction by the presence of spatially-remote Pt can be explained by the spillover of dissociated hydrogen from Pt clusters onto the Mg(Al)O_x support surface. The spilled-over H migrates between the physically mixed grains of Mg(Al)O_x and Mg(Ga)(Al)O_x and then reduces Ga^{3+} species. This mechanism of long-range transport of spilled-over hydrogen must also be involved in Ga reduction and subsequent Pt–Ga cluster formation on Pt–Ga/Mg(Ga)(Al)O_x catalysts. However, conflicting reports on the occurrence of hydrogen spillover necessitate additional consideration before unambiguously concluding that hydrogen spillover explains these XAS results.

In a recent critical review[28] of possible mechanisms of hydrogen transport over the surfaces of catalysts and functional materials, Prins defined spill-over as ''the transport of a species, adsorbed or formed on a surface, to another surface, which does not adsorb or form this species under the same conditions''. It is generally accepted that H_2 dissociatively chemisorbs on Pt surfaces, making Pt cluster surfaces H-rich. The fact that Ga does not reduce in Mg(Ga)(Al)O_x in the absence of Pt suggests that the surface of Ga-incorporated support is rather H-poor (see below), but Ga reduction does take place in the presence of Pt within the same physical mixture. This necessitates a long-range net transport of dissociated H from the H-rich Pt cluster surfaces towards H-poor Mg(Al)O_x, followed by its migration towards Mg(Ga)(Al)O_x to reduce Ga. Such net H-transport from Pt to Mg(Al)O_x indicates H-spillover at the boundary between Pt clusters and the non-reducible Mg(Al)O_x support.

Prins points out that spillover onto non-reducible supports is energetically unfavorable and therefore slow or unlikely.[28] Other mechanisms have been suggested to explain the apparent H-spillover effect. In the present context, these alternatives include the migration of hydrogen-dissociating Pt species[57,58] over the support surface towards Ga^{3+}, the migration of Ga^{3+} towards Pt, and hydrocarbon contamination of the catalyst.[28] The former two possibilities are inconsistent with high angle annular dark field scanning transmission electron microscopy (HAADF-STEM) imaging and energy dispersive X-ray (EDX) mapping experiments performed on the physical mixture of Pt/Mg(Al)O_x and Mg(Ga)(Al)O_x. Fig. 3 shows a HAADF-STEM (Z-contrast) image of two distinct, spatially separated

$Mg(Ga)(Al)O_x$ and $Pt/Mg(Al)O_x$ grains after TPR treatment to 650 °C. The inset EDX elemental maps clearly show a Ga-rich but Pt-poor $Mg(Ga)(Al)O_x$ grain next to a Pt-rich but Ga-poor $Pt/Mg(Al)O_x$ grain. Based on the extracted EDX spectra, no Pt (Ga) is detected on $Mg(Ga)(Al)O_x$ ($Pt/Mg(Al)O_x$) after TPR to 650 °C. This evidences that neither Pt nor Ga species migrate towards other grains to induce Ga reduction during TPR treatment. In addition, Ga K and Pt L_{III} edge XANES spectra of the reduced physical mixture confirm that Pt and Ga do not contact to reduce Ga, since then Pt–Ga alloying should be observed. Hydrocarbon contamination that could account for the apparent H-transport can also be excluded, since all samples were calcined for 4 hours at 650 °C. High temperature calcination burns off all carbonaceous species remaining after $Pt(acac)_2$ precursor impregnation, and no hydrocarbons were used during the experiments. It should be noted that the Somorjai group[30] recently suggested the occurrence of H-spillover from Pt across non-reducible SiO_2 support to Co during CO_2 methanation.

To substantiate the involvement of H-spillover, the interaction of H_2 with the $Mg(Al)O_x$, $Mg(Ga)(Al)O_x$, and $Pt/Mg(Al)O_x$ materials at 650 °C was characterized using Temporal Analysis of Products (TAP) pulse-response experiments[59–61] (see Methods and ESI† for experimental and data analysis details). Each material was first reduced for 20 minutes in a flow of H_2 at 650 °C and then, after a 20 minute evacuation to the background pressure of 10^{-5} Pa, was subjected to a series of very small (10^{-8} mol) and short pulses of a 1 : 1 H_2/He mixture. The exit-flow rates of

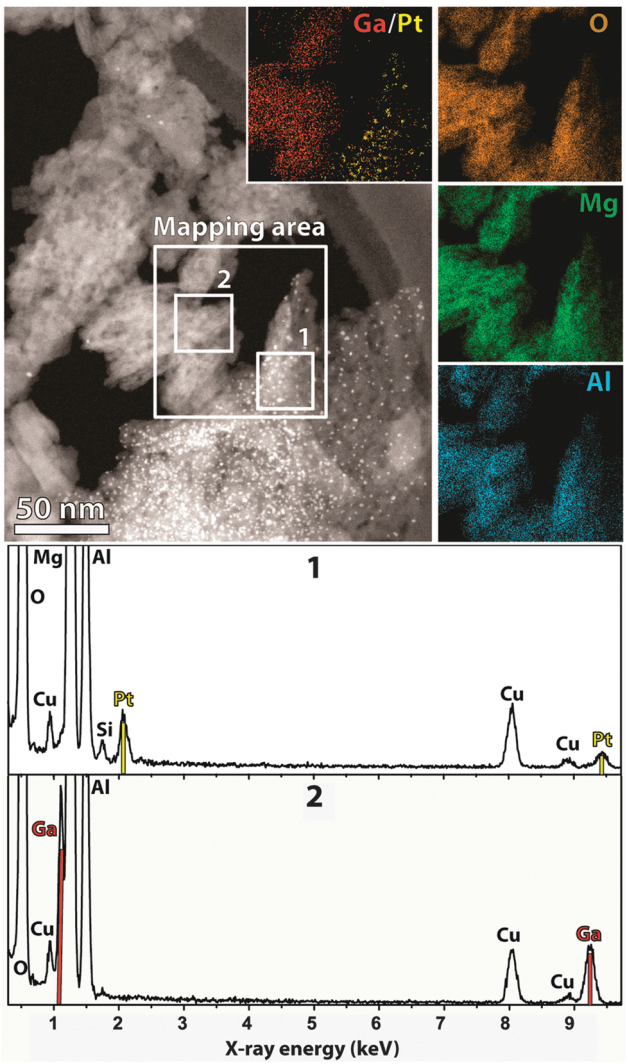

Fig. 3 HAADF-STEM image, EDX maps and EDX spectra of the physical mixture, *i.e.* $Pt/Mg(Al)O_x$ + $Mg(Ga)(Al)O_x$, after H_2/He TPR to 650 °C. The white rectangle in the HAADF-STEM image indicates the region mapped by STEM-EDX. EDX maps for Ga, Pt, O, Mg and Al are inset. Extracted EDX spectra from regions 1 and 2 indicated in the HAADF-STEM image are plotted below. The red lines indicate the positions of the main peaks for Ga (L at 1.099 keV & K_α at 9.242 keV) and the yellow lines indicate the positions of the main peaks for Pt (M_α at 2.050 keV & L_α at 9.435 keV).

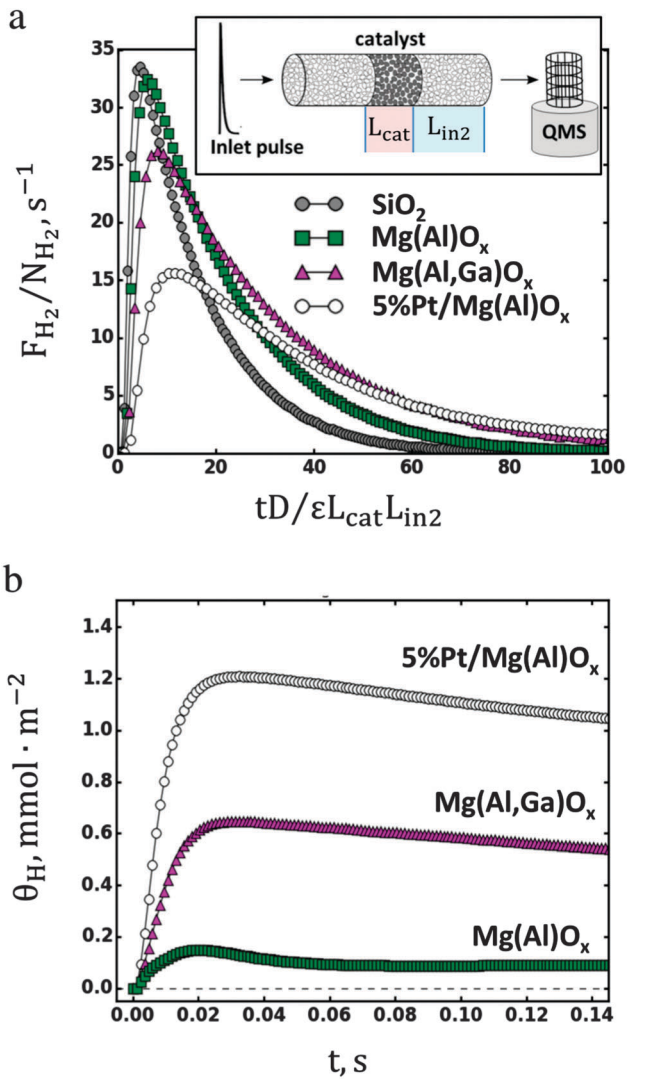

Fig. 4 TAP pulse-response experiments at 650 °C; (a) H_2 exit-flow rates in 1 s^{-1} normalized by the injected amount N_{H_2} as a function of dimensionless time normalized by the effective diffusivity D in m^2 s^{-1}, the bed porosity ε, the catalyst length L_{cat} in m, and the length of the second inert zone L_{in2} in m. The curves are compared for different materials: SiO_2 (●), $Mg(Al)O_x$ (■), $Mg(Ga)(Al)O_x$ (▲), and $Pt/Mg(Al)O_x$ (○). The inset conceptually depicts a TAP experiment; (b) H-uptakes in mmol m^{-2} on different materials *versus* time.

H_2 pulsed at 650 °C over different materials are reported in Fig. 4a. The scaled abscissa of the plot in Fig. 4a represents dimensionless time, which is defined as $\tau = tD/\varepsilon L_{cat}L_{in2}$, where t (s) is real time, D ($m^2\ s^{-1}$) is an effective diffusion coefficient, ε is bed porosity (–), L_{cat} (m) and L_{in2} (m) are the lengths of the catalyst zone and the inert zone downstream of the catalyst zone, respectively. The ordinate of the plot represents the exit-flow rate divided by the amount of admitted molecules. Such scaling of the experimental curves takes into account all transport- and geometry-related variations between different experiments and allows one to focus only on the chemistry-related effects. The hydrogen response over a bed of inert SiO_2 particles represents the diffusion-only process in the absence of chemical interactions.

In experiments with the actual materials investigated in this study, the same SiO_2 particles were used to pack the two inert zones upstream and downstream of the catalytic sample. As evident from Fig. 4a, the other three curves increasingly deviate from the SiO_2 curve in the following order $Mg(Al)O_x$ < $Mg(Ga)(Al)O_x$ < $Pt/Mg(Al)O_x$, suggesting that all three materials adsorb hydrogen at 650 °C. The peak value decreases and shifts to the right, while the tail rises. This behavior is indicative of the increasing life-time of reversibly dissociated H_2 on the catalyst surface. Other factors which could account for the increased delay of hydrogen response include side reactions leading to additional products and additional transport limitations, *e.g.* due to intra-particle pore diffusion. However, these factors are excluded since (1) no other products evolved from the catalyst and (2) the simultaneously recorded He response conformed to Knudsen diffusion through the bed with no pore diffusion.

Based on the exit-flow rates, the instantaneous surface coverage of hydrogen on the catalyst (mol_H/m_{cat}^2) was evaluated under the assumption of dissociative chemisorption ($H_2 + 2^* = 2H$), but with no additional kinetic assumptions[59–61] (see Fig. 4b). On all materials, H-coverage achieves a peak value within the first 0.02–0.03 s of the experiment and then slowly decreases due to desorption. The Pt-free $Mg(Al)O_x$ support clearly dissociated H_2 by itself, in agreement with multiple studies evidencing either homolytic or heterolytic H_2 dissociation on defective MgO surfaces.[62,63] A much more substantial coverage is developed on the $Mg(Ga)(Al)O_x$ support. The latter observation is consistent with the intrinsic hydrogen dissociation[64] and alkane dehydrogenation[65] activity of Ga oxide, the inclusions of which may be present within the mixed oxide framework of $Mg(Ga)(Al)O_x$. It is also plausible that isolated Ga sites are responsible for H_2 dissociation. As expected, the coverage on the Pt-containing catalyst was an order of magnitude higher than on the Pt-free $Mg(Al)O_x$ support and at least twice higher than on $Mg(Ga)(Al)O_x$.

Considering all presented findings, we conclude that the reduction and alloying of Pt and Ga during the formation of $Pt–Ga/Mg(Ga)(Al)O_x$ catalysts is mediated primarily by H-species which are dissociatively chemisorbed on Pt nanoparticles and spilled-over onto the support. Although the LDH-derived supports are capable of dissociating hydrogen by themselves, the combined *in situ* XAS and TAP experiments suggest that not all H-species on the support surface contribute equally to the reduction of Ga^{3+}. TAP experiments demonstrate a significant life-time of H on the $Mg(Ga)(Al)O_x$ surface, but *in situ* XANES data reveal that Ga reduction on Pt-free materials is insignificant at 650 °C. At first glance, it appears that Ga reduction is kinetically hindered by the limited ability of the support to form reduction-capable H-species. Only in the presence of Pt does the population of such species on the support surface increase and accelerate Ga reduction.

A more detailed reaction mechanism is proposed to clarify the observations (Fig. 5). $Mg(Ga)(Al)O_x$ supports expose Ga–O

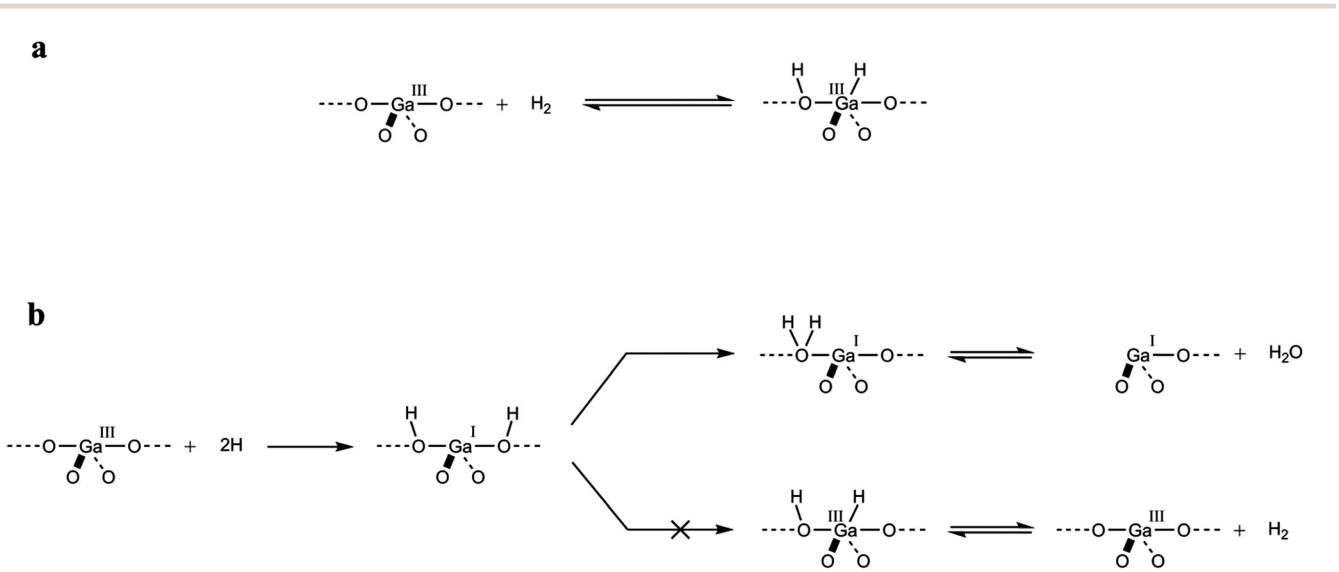

Fig. 5 (a) Reversible H_2 dissociative chemisorption on Ga–O bonds at the Pt-free $Mg(Ga)(Al)O_x$ support, yielding Ga–H hydride and Ga–OH hydroxyl groups at the surface, (b) reaction mechanism for spilled over atomic H species dissociated by Pt(2H), which interact with Ga–O centers at the $Mg(Ga)(Al)O_x$ surface, resulting in partial reduction of Ga^{3+}. The lower route involving Ga–H hydride formation through H-transfer from adjacent Ga–OH hydroxyl groups is kinetically hindered and therefore unlikely to occur.

bonds at the support surface. These Ga–O bonds activate the heterolytic dissociation of H_2, resulting in the formation of Ga–H hydride and Ga–OH hydroxyl groups at the support surface (Fig. 5a).[66] After dissociative chemisorption, the preferred reaction path is to recombine H atoms from Ga–H and Ga–OH groups into H_2 molecules which desorb from the support surface.[66,67] In this way, Ga^{3+} sites reversibly interact with gas phase H_2, but are recovered without undergoing significant Ga reduction. This is in line with both TAP and XANES results: TAP clearly shows significant H chemisorption on the Mg(Ga)(Al)O_x surface at 650 °C compared to Mg(Al)O_x, while *in situ* Ga K edge XANES during H_2 TPR of Mg(Ga)(Al)O_x shows no significant Ga reduction.

In the presence of Pt, the Pt cluster surface promotes the homolytic dissociation of gas phase H_2 into atomic H.[28] These activated H atoms spill over to the support, migrate across the support surface and undergo long-range transport. At Ga–O centers, H atoms likely form Ga–OH hydroxyl groups, rather than Ga–H hydride bonds, as the latter are unfavored.[67] Indeed, Liu *et al.*[67] and Copéret[66] show that Ga–H hydride formation through H-transfer from adjacent Ga–OH hydroxyl groups is kinetically hindered and therefore slow. As a consequence, OH groups are expected to surround Ga, resulting in the reduction of Ga^{3+} into Ga^{1+} – as described by Copéret (Fig. 5b).[66] At high temperature, the dominant mechanism consists of H-transfer from one Ga–OH group to an adjacent one, resulting in H_2O formation and subsequent desorption (Fig. 5b).[66,67] This process does not recover the original Ga^{3+}–O surface sites due to a net (partial) reduction of Ga^{3+} into Ga^{1+} as a consequence of H_2O removal. These results are in agreement with *in situ* Ga K edge XANES results recorded during H_2 TPR of Pt-containing catalysts, namely Pt/Mg(Al)O_x + Mg(Ga)(Al)O_x and Pt/Mg(Ga)(Al)O_x, in which a partial reduction of Ga^{3+} cations is observed (Fig. 1b and c).

Besides the nature and behavior of hydrogen, the range of metal migration during the reduction process also plays an important role in the bimetallic catalyst formation. As evidenced by XANES and TEM results for the physical mixture, partially reduced $Ga^{\delta+}$ species possess limited mobility at 650 °C, inhibiting further Ga reduction into Ga^0 and concomitant Pt–Ga alloying. Complementary experiments at 750 °C demonstrate that Pt–Ga alloying does occur when the mobility of partially reduced $Ga^{\delta+}$ species is increased at higher temperatures. In Fig. 6a, the Pt L_{III} edge XANES white line height is plotted *versus* the edge energy shift $(E(\mu x = 1)_{T=t} - E(\mu x = 1)_{T=RT})$ during reduction treatment for the following cases: (1) H_2 TPR of a Ga-free Pt/Mg(Al)O_x reference up to 650 °C (red dashed line), (2) H_2 TPR of Pt/Mg(Ga)(Al)O_x bimetallic catalyst up to 650 °C (green full line), (3) H_2 TPR of the physical mixture Pt/Mg(Al)O_x + Mg(Ga)(Al)O_x up to 650 °C (blue full line), and (4) H_2 TPR of the same the physical mixture from 650 °C up to 750 °C (blue dotted line).

Similar to the Pt/Mg(Al)O_x reference, the bimetallic catalyst Pt/Mg(Ga)(Al)O_x displays a white line height decrease typical of Pt reduction. In addition, H_2 TPR of Pt/Mg(Ga)(Al)O_x induces a strong edge shift to higher energies, implying Pt–Ga alloying of $Ga^{\delta+}$ with nearby Pt. The physical mixture only undergoes

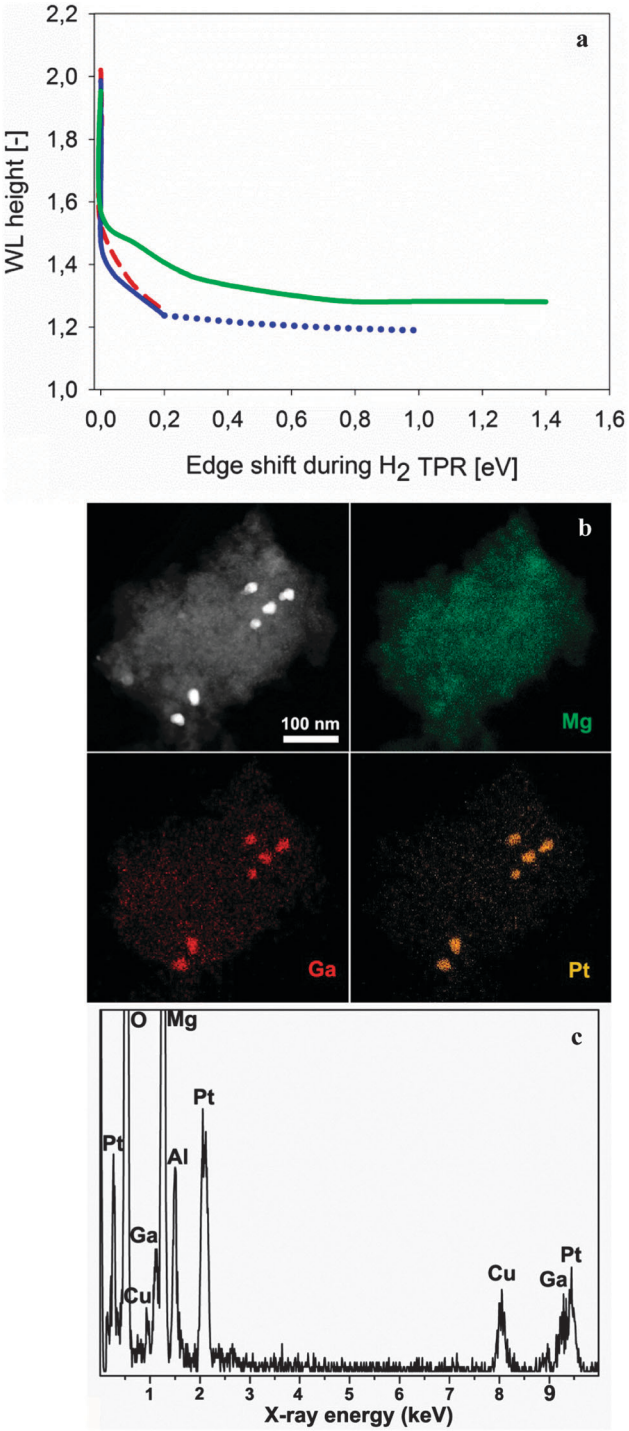

Fig. 6 (a) Pt L_{III} edge white line height as a function of the edge shift during H_2 TPR for (green full line) Pt/Mg(Ga)(Al)O_x to 650 °C, (blue full line) Pt/Mg(Al)O_x + Mg(Ga)(Al)O_x to 650 °C and (blue dotted line) Pt/Mg(Al)O_x + Mg(Ga)(Al)O_x from 650 °C to 750 °C. The white line-edge shift evolution for a Pt/Mg(Al)O_x reference is also displayed for comparison (dashed red line); (b) HAADF-STEM image, EDX maps and (c) EDX spectrum of the physical mixture, *i.e.* Pt/Mg(Al)O_x + Mg(Ga)(Al)O_x, after H_2 TPR to 750 °C.

Pt phase reduction during H_2 TPR to 650 °C (blue full line), similar to H_2 TPR of Pt/Mg(Al)O_x (red dashed line). In contrast, H_2 TPR of the physical mixture from 650 °C to 750 °C results in

a strong edge shift to higher energies. $Ga^{\delta+}$ species are thus thermally activated to overcome the activation barrier of migration towards spatially remote Pt, where they are further reduced to Ga^0 and alloy with Pt. Indeed, EDX mapping experiments performed on a grain of the physical mixture being reduced to 750 °C in H_2 confirms that both Pt and Ga atoms are present on the same grain. In addition, both the Pt and Ga concentrations are increased at specific locations on this grain, proving that Pt–Ga alloying is established after H_2 TPR to 750 °C. An increase of the temperature from 650 °C to 750 °C in H_2 allows switching from a hydrogen transport dominated regime in which Ga migration is limited to short-range transport, towards a regime in which both hydrogen and Ga transport are kinetically allowed.

In the bimetallic catalysts investigated, an energy gain from alloying with vicinal Pt allows $Ga^{\delta+}$ to overcome the activation barrier towards Ga^0 at 650 °C. For this reason, the H_2 reduction process of framework incorporated Ga^{3+} cations which eventually alloy with Pt during the formation of Pt–Ga/Mg(Ga)(Al)O_x catalysts consists of three consecutive steps: (1) partial reduction of Ga^{3+} into $Ga^{\delta+}$ by Pt-dissociated hydrogen, (2) support surface migration of partially reduced, moderately mobile $Ga^{\delta+}$ species towards Pt clusters, followed by (3) complete reduction of $Ga^{\delta+}$ to metallic Ga^0 on the condition of simultaneous stabilization of Ga^0 in a Pt–Ga alloy.

Conclusions

Novel mechanistic details were elucidated for H-spillover, metal reduction, and metal mobility involved in the formation of bimetallic Pt–Ga catalysts on LDH-derived supports. Non-equal reductive ability of different forms of dissociated H_2 was suggested, motivating further research and more detailed characterization of surface-bound hydrogen species on the surfaces of mixed oxides. These results suggest that hydrogen spillover from catalytic metal nanoparticles onto non-reducible supports may play a decisive role not only in the catalytic reactions themselves, but also in shaping the ''working state'' of the catalyst during the pretreatment. These results boost the opportunity to influence the formation and reactivity of catalysts supported on non-reducible oxides derived from LDHs by taking advantage of the H spill-over and its consecutive migration.

Acknowledgements

This work was supported by the Fund for Scientific Research Flanders (FWO: G.0209.11), the 'Long Term Structural Methusalem Funding by the Flemish Government', the IAP 7/05 Interuniversity Attraction Poles Programme – Belgian State – Belgian Science Policy, and the Fund for Scientific Research Flanders (FWO-Vlaanderen) in supplying financing of beam time at the DUBBLE beam line of the ESRF and travel costs and a post-doctoral fellowship for S.T. The authors acknowledge the assistance from D. Banerjee (XAS campaign 26-01-979) at DUBBLE. E. A. Redekop acknowledges the Marie Curie International Incoming Fellowship granted by the European Commission (Grant Agreement No. 301703). The authors also express their gratitude to V. Bliznuk for acquisition of the TEM images.

References

1 B. C. Gates, *Chem. Rev.*, 1995, **95**, 511.
2 S. Muratsugu, S. Kityakam, F. Wang, N. Ishiguro, T. Kamachi, K. Yoshizawa, O. Sekizawa, T. Uruga and M. Tada, *Phys. Chem. Chem. Phys.*, 2015, **17**, 24791.
3 F. Shojaei, M. Mousavi, F. Nazari and F. Illas, *Phys. Chem. Chem. Phys.*, 2015, **17**, 3659.
4 W. Yu, M. D. Porosoff and J. G. Chen, *Chem. Rev.*, 2012, **112**, 5780.
5 Y. J. Ma, R. F. Wang, H. Wang, V. Linkov and S. Li, *Phys. Chem. Chem. Phys.*, 2014, **16**, 3593.
6 H. Feng, J. A. Libera, P. C. Stair, J. T. Miller and J. W. Elam, *ACS Catal.*, 2011, **1**, 665.
7 B. J. O'Neill, D. H. K. Jackson, J. Lee, C. Canlas, P. C. Stair, C. L. Marshall, J. W. Elam, T. F. Kuech, J. A. Dumesic and G. W. Huber, *ACS Catal.*, 2015, **5**, 1804.
8 Y. Xia, Y. Xiong, B. Lim and S. E. Skrabalak, *Angew. Chem., Int. Ed.*, 2009, **48**, 60.
9 C. N. Satterfield, *Heterogeneous Catalysis in Industrial Practice*, Mcgraw-Hill, New York, 1991.
10 F. Basile, L. Basini, G. Fornasari, M. Gazzano, F. Trifirò and A. Vaccari, *Chem. Commun.*, 1996, 2435.
11 B. F. Sels, D. E. De Vos and P. A. Jacobs, *Catal. Rev.*, 2001, **43**, 443.
12 Z. P. Xu, J. Zhang, M. O. Adebajo, H. Zhang and C. Zhou, *Appl. Clay Sci.*, 2011, **53**, 139.
13 L. He, Y. Huang, A. Wang, X. Wang, X. Chen, J. J. Delgado and T. Zhang, *Angew. Chem., Int. Ed.*, 2012, **51**, 6191.
14 B. Ballarin, R. Seeber, D. Tonelli and A. Vaccari, *J. Electroanal. Chem.*, 1999, **463**, 123.
15 Q. Xiao, Z. Liu, A. Bo, S. Zavahir, S. Sarina, S. Bottle, J. D. Riches and H. Zhu, *J. Am. Chem. Soc.*, 2015, **137**, 1956.
16 S. Walspurger, P. D. Cobden, O. V. Safonova, Y. Wu and E. J. Anthony, *Chem. – Eur. J.*, 2010, **16**, 12694.
17 C. Aguzzi, P. Cerezo, C. Viseras and C. Caramella, *Appl. Clay Sci.*, 2007, **36**, 22.
18 A. I. Khan and D. O'Hare, *J. Mater. Chem.*, 2002, **12**, 3191.
19 A. Virnovskaia, S. Jørgensen, J. Hafizovic, Ø. Prytz, E. Kleimenov, M. Hävecker, H. Bluhm, A. Knop-Gericke, R. Schlögl and U. Olsbye, *Surf. Sci.*, 2007, **601**, 30.
20 A. Virnovskaia, S. Morandi, E. Rytter, G. Ghiotti and U. Olsbye, *J. Phys. Chem. C*, 2007, **111**, 14732.
21 A. Virnovskaia, E. Rytter and U. Olsbye, *Ind. Eng. Chem. Res.*, 2008, **47**, 7167.
22 V. Galvita, G. Siddiqi, P. Sun and A. T. Bell, *J. Catal.*, 2010, **271**, 209.
23 F. Basile, G. Fornasari, M. Gazzano and A. Vaccari, *Appl. Clay Sci.*, 2000, **16**, 185.
24 S. Velu, K. Suzuki, M. Okazaki, T. Osaki, S. Tomura and F. Ohashi, *Chem. Mater.*, 1999, **11**, 2163.

25 S. Ribet, D. Tichit, B. Coq, B. Ducourant and F. Morato, *J. Solid State Chem.*, 1999, **142**, 382.
26 A. Ota, E. L. Kunkes, I. Kasatkin, E. Groppo, D. Ferri, B. Poceiro, R. M. Navarro Yerga and M. Behrens, *J. Catal.*, 2012, **293**, 27.
27 S. Kühl, A. Tarasov, S. Zander, I. Kasatkin and M. Behrens, *Chemistry*, 2014, **20**, 3782.
28 R. Prins, *Chem. Rev.*, 2012, **112**, 2714.
29 R. Prins, V. K. Palfi and M. Reiher, *J. Phys. Chem. C*, 2012, **116**, 14274.
30 S. K. Beaumont, S. Alayoglu, C. Specht, N. Kruse and G. A. Somorjai, *Nano Lett.*, 2014, **14**, 4792.
31 J. Im, H. Shin, H. Jang, H. Kim and M. Choi, *Nat. Commun.*, 2014, **5**, 3370.
32 E. S. Shpiro, D. P. Shevchenko, O. P. Tkachenko and R. V. Dmitriev, *Appl. Catal., A*, 1994, **107**, 147.
33 J. J. H. B. Sattler, I. D. Gonzalez-Jimenez, L. Luo, B. A. Stears, A. Malek, D. G. Barton, B. A. Kilos, M. P. Kaminsky, T. W. G. M. Verhoeven, E. J. Koers, M. Baldus and B. M. Weckhuysen, *Angew. Chem., Int. Ed.*, 2014, **53**, 9251.
34 P. Sun, G. Siddiqi, M. Chi and A. T. Bell, *J. Catal.*, 2010, **274**, 192.
35 G. Siddiqi, P. Sun, V. Galvita and A. T. Bell, *J. Catal.*, 2010, **274**, 200.
36 P. Sun, G. Siddiqi, W. C. Vining, M. Chi and A. T. Bell, *J. Catal.*, 2011, **282**, 165.
37 M. Filez, E. A. Redekop, H. Poelman, V. V. Galvita, M. Meledina, S. Turner, G. Van Tendeloo, C. Detavernier and G. B. Marin, *Catal. Sci. Technol.*, 2015, DOI: 10.1039/C5CY01274K.
38 E. A. Redekop, V. V. Galvita, H. Poelman, V. Bliznuk, C. Detavernier and G. B. Marin, *ACS Catal.*, 2014, **4**, 1812.
39 M. Filez, E. A. Redekop, H. Poelman, V. V. Galvita, R. K. Ramachandran, J. Dendooven, C. Detavernier and G. B. Marin, *Chem. Mater.*, 2014, **26**, 5936.
40 M. Filez, E. A. Redekop, H. Poelman, V. V. Galvita and G. B. Marin, *Anal. Chem.*, 2015, **87**, 3520.
41 O. B. Belskaya, N. N. Leont'eva, T. I. Gulyaeva, V. A. Drozdov, V. P. Doronin, V. I. Zaikovskii and V. A. Likholobov, *Kinet. Catal.*, 2011, **52**, 761.
42 B. Dragoi, A. Ungureanu, A. Chirieac, C. Ciotonea, C. Rudolf, S. Royer and E. Dumitriu, *Appl. Catal., A*, 2015, **504**, 92.
43 S. Nikitenko, A. M. Beale, A. M. J. van der Eerden, S. D. M. Jacques, O. Leynaud, M. G. O'Brien, D. Detollenaere, R. Kaptein, B. M. Weckhuysen and W. Bras, *J. Synchrotron Radiat.*, 2008, **15**, 632.
44 V. Martis, A. M. Beale, D. Detollenaere, D. Banerjee, M. Moroni, F. Gosseline and W. Bras, *J. Synchrotron Radiat.*, 2014, **21**, 462.
45 B. Ravel and M. Newville, *J. Synchrotron Radiat.*, 2005, **12**, 537.
46 D. C. Koningsberger, B. L. Mojet, G. E. van Dorssen and D. E. Ramaker, *Top. Catal.*, 2000, **10**, 143.
47 L. S. Hsu, G. Y. Guo, J. D. Denlinger and J. W. Allen, *Phys. Rev. B: Condens. Matter Mater. Phys.*, 2001, **63**, 155105.
48 R. Giedigkeit, Z. Hu and Y. Grin, XANES study on the intermetallic compounds PdGa and PtGa, two representatives of the FeSi structure: http://hasyweb.desy.de/science/annual_reports/2002_report/part1/contrib/41/6974.pdf.
49 E. Bus and J. A. van Bokhoven, *J. Phys. Chem. C*, 2007, **111**, 9761.
50 K. Nishi, K.-I. Shimizu, M. Takamatsu, H. Yoshida, A. Satsuma, T. Tanaka, S. Yoshida and T. Hattori, *J. Phys. Chem. B*, 1998, **102**, 10190.
51 G. D. Meitzner, E. Iglesia, J. E. Baumgartner and E. S. Huang, *J. Catal.*, 1993, **140**, 209.
52 K. J. Chao, A. C. Wei, H. C. Wu and J. F. Lee, *Microporous Mesoporous Mater.*, 2000, **35–36**, 413.
53 R. Carli, C. L. Bianchi, R. Giannantonio and V. Ragaini, *J. Mol. Catal.*, 1993, **83**, 379.
54 G. L. Price and V. Kanazirev, *J. Catal.*, 1990, **126**, 267.
55 G. L. Price and V. Kanazirev, *J. Mol. Catal.*, 1991, **66**, 115.
56 V. Kanazirev, R. Piffer and H. Forster, *J. Mol. Catal.*, 1991, **69**, L15.
57 H. Y. Liu, W. A. Chiou, G. Fröhlich and W. H. Sachtler, *Top. Catal.*, 2000, **10**, 49.
58 M. Filez, H. Poelman, R. K. Ramachandran, J. Dendooven, K. Devloo-Casier, E. Fonda, C. Detavernier and G. B. Marin, *Catal. Today*, 2014, **229**, 2.
59 J. T. Gleaves, G. S. Yablonskii, P. Phanawadee and Y. Schuurman, *Appl. Catal., A*, 1997, **160**, 55.
60 J. T. Gleaves, G. Yablonsky, X. Zheng, R. Fushimi and P. L. Mills, *J. Mol. Catal.*, 2010, **315**, 108.
61 G. S. Yablonsky, D. Constales, S. O. Shekhtman and J. T. Gleaves, *Chem. Eng. Sci.*, 2007, **62**, 6754.
62 M. Boudart, A. Delbouille, E. G. Derouane, V. Indovina and A. B. Walters, *J. Am. Chem. Soc.*, 1972, **94**, 6622.
63 E. Knözinger, K.-H. Jacob and P. Hofmann, *J. Chem. Soc., Faraday Trans.*, 1993, **89**, 1101.
64 S. E. Collins, M. A. Baltanas and A. L. Bonivardi, *Langmuir*, 2005, **21**, 962.
65 B. Zheng, W. Hua, Y. Yue and Z. Gao, *J. Catal.*, 2005, **232**, 143.
66 C. Copéret, *Chem. Rev.*, 2010, **110**, 656.
67 Y. Liu, Z. Hua Li, J. Lu and K.-N. Fan, *J. Phys. Chem. C*, 2008, **112**, 20382.